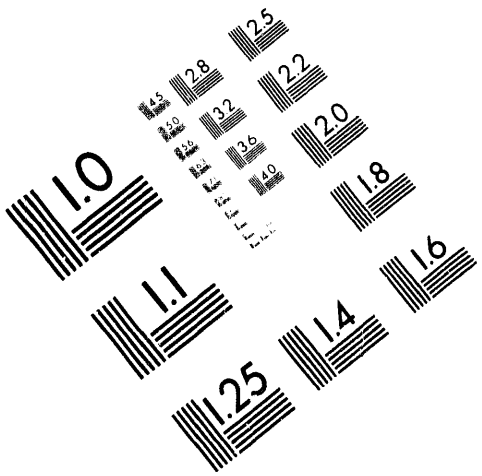

Association for Information and Image Management

1100 Wayne Avenue, Suite 1100
Silver Spring, Maryland 20910

301/587-8202

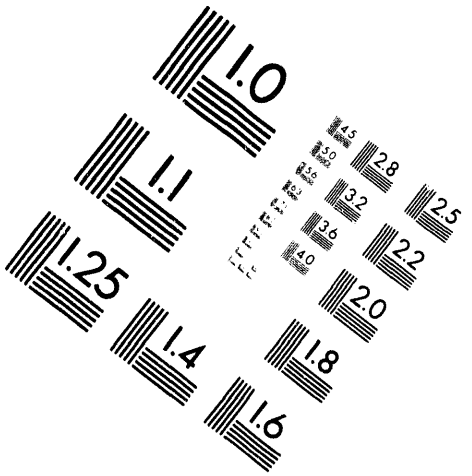

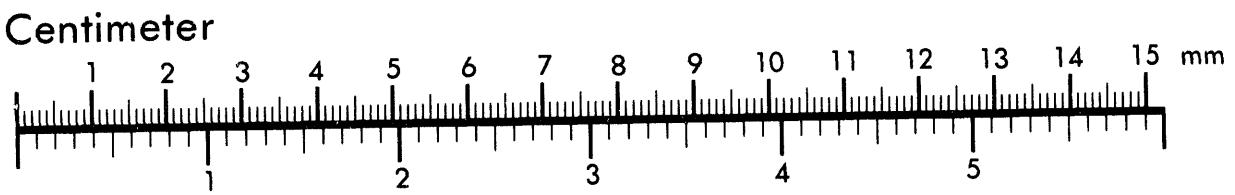

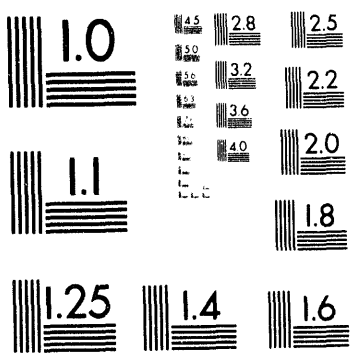

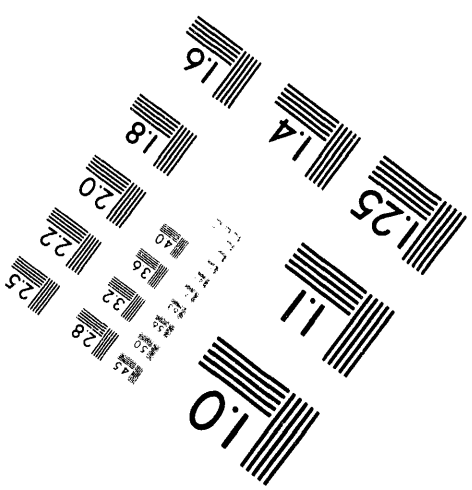

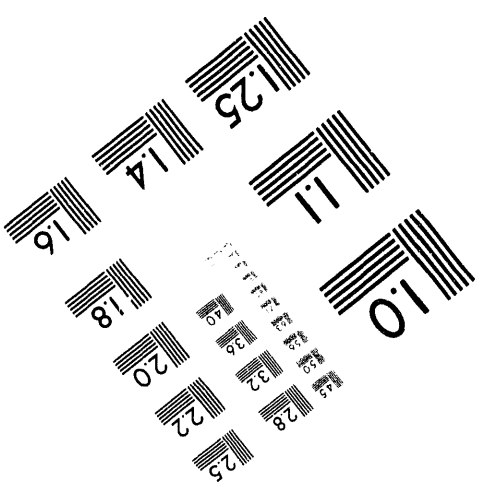

1 of 1

2

Conf-940553--15

UCRL-JC-114790
PREPRINT

Dispersivity in Heterogeneous Permeable Media

Dwayne A. Chesnut

This paper was prepared for submittal to the
American Nuclear Society
International High Level Radioactive Waste Management Conference
Las Vegas, NV
May 22 - 26, 1994

January 1994

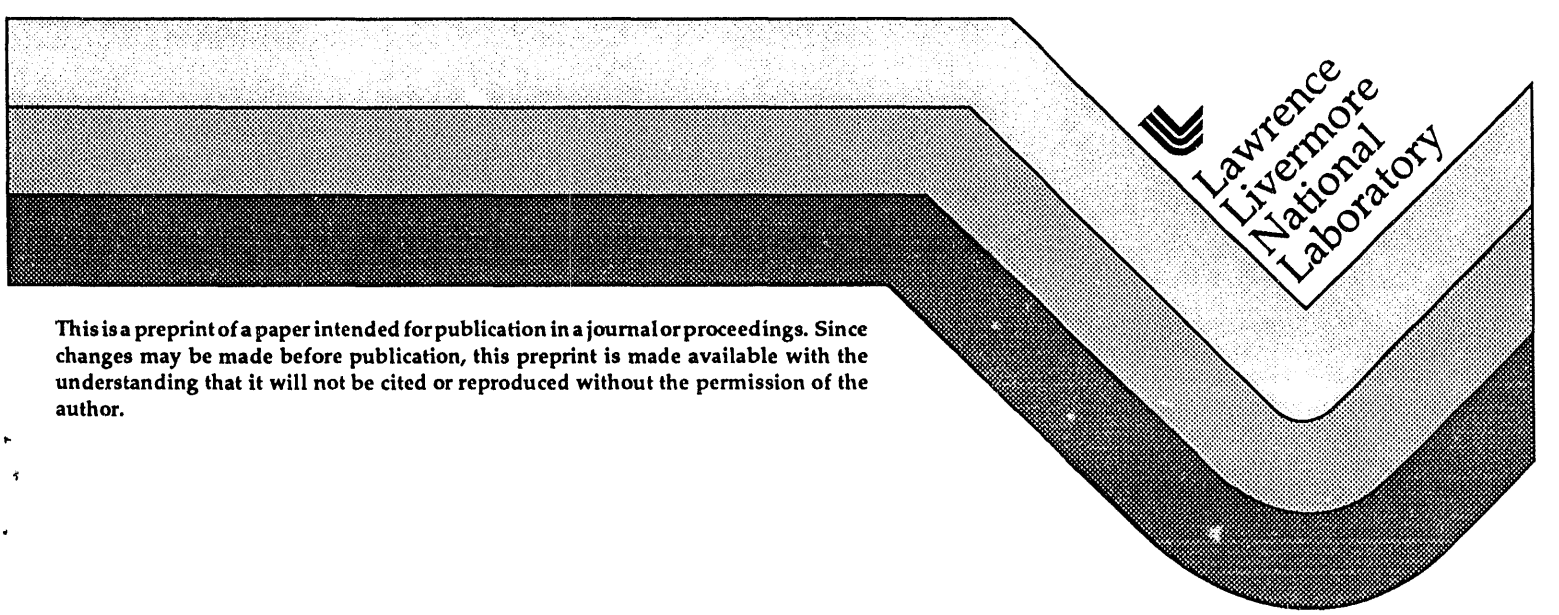

DISPERSIVITY IN HETEROGENEOUS PERMEABLE MEDIA

Dwayne A. Chesnut
Lawrence Livermore National Laboratory
P. Box 808, L-202
Livermore, CA 94550
(510)423-5053

ABSTRACT

When one fluid displaces another through a one-dimensional porous medium, the composition changes from pure displacing fluid at the inlet to pure displaced fluid some distance downstream. The distance over which an arbitrary percentage (typically 80%) of this change occurs is defined as the mixing zone length, which increases with increasing average distance traveled by the displacement front. Alternatively, for continuous injection, the mixing zone size can be determined from a breakthrough curve as the time required for the effluent displacing fluid concentration to change from, say, 10% to 90%. In classical dispersion theory, the mixing zone grows in proportion to the square root of the mean distance traveled, or, equivalently, to the square root of the mean breakthrough time.

In a multi-dimensional heterogeneous medium, especially at field scales, the size of the mixing zone grows almost linearly with mean distance or travel time. If an observed breakthrough curve is forced to fit the classical theory, the resulting effective dispersivity, instead of being constant, also increases almost linearly with the spatial or temporal scale of the problem. This occurs because the heterogeneity in flow properties creates a corresponding velocity distribution along the different flow pathways from the inlet to the outlet of the system. Mixing occurs mostly at the outlet, or wherever the fluid is sampled, rather than within the medium.

In this paper, we consider the effects of this behavior on radionuclide or other contaminant migration. In a limiting case, the breakthrough curve is given by a log-normal cumulative probability function of time, with parameters t_b (a characteristic breakthrough time) and σ (the standard deviation in the natural logarithm of the breakthrough time). The apparent mixing zone width increases in exact proportion to the distance traveled, with the proportionality "constant" given by a function of σ. For small σ, the breakthrough curve resulting from releasing a narrow pulse at time zero has a sharp peak near $t = t_b$. As σ increases (corresponding to increasing heterogeneity), the location of the peak shifts monotonically to smaller values of t, and the peak concentration at first decreases, then *increases* rapidly as the location of the peak moves toward zero time, indicating that there may be a limit to the dilution effect expected with increasing "dispersion." Concurrently, an increasing fraction of the total contaminant mass is produced at early time. Both the increased peak concentrations and the increased early total mass production are consistent with the intuitive concept of "fast paths" for radionuclide transport.

I. INTRODUCTION

At the laboratory scale, the shape of the composition profile between pure displaced fluid and pure displacing fluid is closely approximated by an appropriate solution to a form of the diffusion equation (the convection-dispersion equation, or CDE), with a longitudinal dispersion coefficient in place of the diffusion constant.

Experimental data for laboratory-scale displacements are well represented by assuming that the dispersion coefficient is equal to the product of the fluid velocity and a constant, characteristic of the porous medium, known as the *dispersivity*.[1] The width of the mixing zone grows in proportion to the *square root* of the average distance traveled by the displacement front.[2]

At field scales, an increasing number of examples indicate that the width of the mixing zone grows in proportion to the p^{th} power of the distance traveled, where p is greater than 1/2, and may approach unity. If field breakthrough curves are forced to fit the convection-dispersion solution, it is found that the effective dispersivity, rather than approaching a constant value

characteristic of the medium, increases almost linearly with the scale of the problem.[3,4]

Apparently, the mixing zone width is controlled by the variation in fluid velocity from point to point within the medium, which in turn is governed by the heterogeneity in permeability and porosity, and its spatial correlation structure. Hewett[5] calls this behavior *velocity dispersion*, in contrast to the classical process of *gradient dispersion* controlled by concentration gradients. In the latter case, the fluids actually mix within the medium, whereas in the former, mixing occurs primarily as a result of sampling at an outflow boundary, such as a well.

In this paper, we consider the effects of velocity dispersion on radionuclide or other contaminant migration. In a limiting case, velocity dispersion can be represented by a log-normal distribution of fluid flux crossing a surface perpendicular to the principal direction of flow. Under this approximation, both the normalized concentration profile and the breakthrough curve of a contaminant (introduced as a unit step function at time 0 at the inflow boundary of the system) will be given by log-normal cumulative probability functions. Each function requires only two parameters: the average breakthrough time, t_b (for concentration vs. time) or $\langle x \rangle$ (for concentration vs. distance), and the standard deviation in the natural logarithm of the breakthrough time, σ. The apparent mixing zone width increases in exact proportion to the distance traveled, with the proportionality "constant" given by a function of σ.

II. MATHEMATICAL DEVELOPMENT

Chesnut, Cox, and Lasaki[6] presented a model for waterflooding petroleum reservoirs in porous sedimentary rock, based on earlier unpublished work by Chesnut,[7] in which the flow paths from injection to production wells are treated as a collection of independent linear elements. Effects of heterogeneity were incorporated by assigning a log-normal permeability distribution to these elements and integrating the displacement behavior over this distribution. Recently, Chesnut applied similar concepts to define more precisely the concept of groundwater travel time arising in US regulations on nuclear waste repository sites,[8] and to develop a model for the rate of extraction of volatile organic compounds from the vadose zone.[9]

Neretnieks[10] and his colleagues have for a number of years been developing similar conceptual and mathematical models of "stratified" or "channel" flow and transport in fractured crystalline rock, principally in connection with the safety assessment of the Swedish nuclear waste repository concept. The thought experiment underlying this approach is described by Neretnieks: "...fissures act as independent channels with no mixing occurring between them. At the inlet end of the channels a tracer can be introduced. This is done simultaneously in all fissures. At some distance downstream the fluid from all channels is collected and mixed. The [resulting] concentration is measured over time ..." A plot of this concentration versus time from the start of tracer injection represents the breakthrough curve.

Butters and co-workers[11,12] conducted an elaborate experiment in which a bromide ion tracer pulse was applied to a uniformly irrigated 80 m by 80 m square plot of "uniform" soil. After application of the pulse, the infiltrating water was sampled periodically, while continuing to irrigate regularly, at depths of 30, 60, 90, 120, 180, 300, and 450 cm, using 16 clusters of sampling tubes centered on a 4×4 array of 20 m by 20 m squares. In their analyses, they applied both the classical convection-dispersion model and a "log-normal transfer function" model previously proposed by Jury and Sposito.[13]

All of these attempts to represent velocity dispersion rest upon the concept of piston-like displacement in a collection of independent linear systems as a starting point for analyzing more complex behavior. Consequently, in the following section we review some basic ideas on ideal linear displacement.

A. Displacement in a Homogeneous System

Consider first an ideal, one-dimensional, "piston-like" miscible displacement of one fluid by another in a completely homogeneous system, representing one of the independent elements, or flow paths, connecting the inlet with the outlet of the heterogeneous system. The two fluids could be clean water displaced by contaminated water, water free of tracer displaced by traced water, or any pair of distinguishable fluids. We assume, for the i^{th} element, that the water flow rate is

$$q_i = k_i \delta A_i \left(\frac{\Delta P}{\mu L} \right) \qquad (1)$$

In Eq. (1), k_i and δA_i are the permeability and cross-sectional area of element i, respectively, taken to be constant along the flow path; ΔP is the pressure drop across the system, which has length L, and μ is the viscosity. We also define the Darcy flux, u_i, and the water velocity, v_i, by

$$u_i = \left(\frac{q_i}{\delta A_i}\right) \tag{2}$$

$$v_i = \left(\frac{u_i}{\phi_i}\right) \tag{3}$$

The velocity of a non-sorbing, non-reactive species is given by Eq. (3), and hence the location of the water displacement front at a time t after the start of injection is just $x_{Di} = v_i t$. For a reversibly sorbed species (but otherwise non-reactive species) with volumetric sorption coefficient K_i, the frontal velocity is given by

$$v_{si} = \left(\frac{u_i}{\phi_i\left[1+K_i\left(\frac{1-\phi_i}{\phi_i}\right)\right]}\right) \tag{4}$$

Also, the sorbing species displacement front at time t is at a position x_{Dsi} given by

$$x_{Dsi} = v_{si} t = \frac{u_i t}{\phi_i R_i} \tag{5},$$

where the usual definition of the retardation coefficient R_i has been used in Eq. (5) to replace the term involving the volumetric sorption coefficient in the denominator of Eq. (4).

B. Displacement in Heterogeneous Systems

We consider the limit of an infinite number of infinitesimal elements, and set

$$\delta A_i = A\,\mathrm{f}(k)dk, \tag{6}$$

where A is the total area perpendicular to the direction of flow and $\mathrm{f}(k)$ is the probability density function for the permeability.

Sums over the index i become integrals over the permeability distribution. In particular, the total flow through the system is given by

$$q_T = \int_0^\infty \frac{A\Delta P}{\mu L} k\,\mathrm{f}(k)dk = \langle k\rangle \frac{A\Delta P}{\mu L} \tag{7},$$

where $\langle k\rangle$ is the average of k over its distribution $\mathrm{f}(k)$. Note that Eq. (7) can be solved for the factor $(\Delta P)/(\mu L)$, and the result rearranged to obtain

$$u_i \equiv \frac{q_i}{\delta A_i} = \left(\frac{q_T}{A}\right)\left(\frac{k_i}{\langle k\rangle}\right) = \frac{\langle u\rangle k_i}{\langle k\rangle} \tag{8}.$$

Equation (8) merely states that the ratio of Darcy flux in an element to the average Darcy flux is the ratio of the permeability of the element to the average permeability.

However, the average water velocity does not necessarily reduce so nicely. By using Eq. (8) in Eq. (3) and then integrating over the permeability distribution, it can be shown that

$$\langle v\rangle = \left(\frac{\langle u\rangle}{\langle k\rangle}\right)\int_0^\infty \frac{k}{\phi} f(k)dk = \frac{\langle u\rangle}{\langle k\rangle}\left\langle\frac{k}{\phi}\right\rangle \tag{9}.$$

Note that in general ϕ will be a function of k, and that the average of k/ϕ will not be exactly equal to the average of k divided by the average of ϕ. Therefore, the average water particle velocity will not be exactly equal to the average Darcy velocity divided by the average porosity. This point will be re-visited later.

A similar, and perhaps worse, difficulty arises in calculating the average frontal displacement velocity (or position) for a sorbing species. By using similar manipulations on Eq. (4), one can show

$$\begin{aligned}\langle v_s\rangle &= \frac{\langle u\rangle}{\langle k\rangle}\left\langle\frac{k}{\phi[1+K(1-\phi)/\phi]}\right\rangle \\ &= \frac{\langle u\rangle}{\langle k\rangle}\left\langle\frac{k}{\phi R}\right\rangle\end{aligned} \tag{10}$$

Note that the ratio k/(ϕR) may be a complex function of k, as well as of many other variables, such as water chemistry and perhaps, as suggested by Neretnieks *et al.*, even the residence time. Furthermore, in general

$$\frac{\langle u\rangle}{\langle k\rangle}\left\langle\frac{k}{\phi R}\right\rangle \neq \frac{\langle u\rangle}{\langle k\rangle}\left\langle\frac{k}{\phi}\right\rangle\left\langle\frac{1}{R}\right\rangle = \langle v\rangle\left\langle\frac{1}{R}\right\rangle \neq \frac{\langle v\rangle}{\langle R\rangle} \tag{11},$$

so that the average frontal velocity of a sorbing species cannot be represented exactly as the average water velocity divided by an average retardation coefficient.

Now consider a distance x at time t after the start of continuous injection of water at concentration c_0 of some detectable species, initially at zero concentration within the medium. For a sorbing species, Eq. (5), with the aid of Eq. (8), can be written for the position of the displacement front in an infinitesimal element with permeability k:

$$x_{Ds} = \left(\frac{\langle u\rangle}{\langle k\rangle}\right)\left(\frac{t}{\phi R}\right)k \qquad (12).$$

At a fixed x and t, all elements for which $x_{Ds} \geq x$ contain injected water at concentration c_0, while all others contain water at zero concentration. Equivalently, for all k such that

$$k \geq \frac{\langle k\rangle \phi R}{\langle u\rangle}\left(\frac{x}{t}\right) \qquad (13),$$

the concentration is equal to c_0. By introducing the unit step function

$$\begin{aligned} &H(z) \equiv 0, \quad && z < 0; \\ &H(z) \equiv 1, \quad && z \geq 0 \end{aligned} \qquad (14)$$

we can write the concentration as a function of time in terms of the following integrals:

$$c_v(x,t) = \int_0^\infty c_0\, H\left[k - \frac{\langle k\rangle \phi R}{\langle u\rangle}\left(\frac{x}{t}\right)\right] f(k)\,dk \qquad (15)$$

$$c_f(x,t) = \int_0^\infty c_0 \frac{k}{\langle k\rangle} H\left[k - \frac{\langle k\rangle \phi R}{\langle u\rangle}\left(\frac{x}{t}\right)\right] f(k)\,dk \qquad (16).$$

These correspond to two different ways of calculating the average concentration as a function of distance and time. The first integral, Eq. (15), represents a *volumetric* average of the concentration *in situ*, which we could in principal determine by suddenly isolating a slice perpendicular to the flow direction and measuring its average concentration. In practice, this might be observed by an electrical conductivity log when saline water is injected into a fresh water aquifer, or *vice versa*. In the experiment of Butters *et al.*,[12] this average was referred to as the *resident concentration*, and was measured at one value of time by coring the irrigation plot after the experiment was concluded, and then analyzing the core material for bromide content as a function of depth.

The second integral is generally more useful, since it is an average weighted by the flow rates of the channels, and gives the concentration which would be measured in Neretnieks' *gedanken* summarized above. Butters *et al.*[12] called this the *flux concentration*. In practice, it is the function which should be compared to observed breakthrough curves for experiments in which 100% of the injected tracer would eventually be produced at the outflow if the experiment were continued indefinitely. Note that the distinction between volumetric weighting and flow-rate weighting to calculate average concentration arises only in situations in which there is velocity dispersion. In classical dispersion theory, the fluid velocity is uniform.

If the second term in the step function argument were independent of k, then the lower limit of the integrals could be set to a function of time and distance only, instead of zero, and the integrals could then be evaluated with an assumed probability distribution function for k. Unfortunately, as discussed above, this is generally not true. Even for the case of a non-sorbing species, when R is identically unity, the porosity would at least be correlated with k, if not functionally dependent. For now, we shall ignore this complication, and replace the product of porosity and retardation coefficient by its average in order to proceed with the analysis. Some consideration has been given to the correlation between sorption coefficients and permeability by Tompson and Dougherty.[14]

C. Log-Normal Distribution

In addition to neglecting the variation of ϕR with k, we now specialize to the case of a log-normal distribution for k, with the density function completely specified by assigning values to its parameters, $\langle \ln k\rangle$ and σ:

$$f(k) = \frac{1}{k\sigma\sqrt{2\pi}} \exp\left[\frac{-(\ln k - \langle \ln k\rangle)^2}{2\sigma^2}\right] \qquad (17).$$

The parameters $\langle \ln k\rangle$ and σ are, respectively, the mean and standard deviation of the natural logarithm of k.

The integrals given above can now be evaluated, setting $\xi = c/c_0$ and using the lower limit

$$k_L = \frac{\langle k\rangle\langle \phi R\rangle}{\langle u\rangle}\left(\frac{x}{t}\right) \qquad (18);$$

$$\xi_v = 1 - \Phi\left\{\frac{\ln(k_L/\langle k\rangle) + \sigma^2/2}{\sigma}\right\} \qquad (19)$$

$$\xi_f = 1 - \Phi\left\{\frac{\ln(k_L / \langle k \rangle) - \sigma^2/2}{\sigma}\right\} \qquad (20),$$

where $\Phi(z)$ is the normal probability integral of z.

Now consider Eq. (20) for some fixed value of x, which may be taken as the outflow of the system, a compliance boundary, or any other surface of interest for calculating the mass transport of contaminant as a function of time. The argument of the natural logarithm in Eq. (20) can be written as

$$k_L / \langle k \rangle = \frac{x\langle \phi R \rangle / \langle u \rangle}{t} \qquad (21).$$

The numerator of the expression on the right hand side of Eq. (21) has the dimension of time, and will be a constant for a fixed x in a given flow system. We then define the characteristic breakthrough time, t_b:

$$t_b \equiv x\langle \phi R \rangle / \langle u \rangle \qquad (22).$$

For the special case of constant porosity and retardation factor, t_b is equal to x divided by the average frontal velocity, and represents a kind of average breakthrough time. In a completely homogeneous system, the normalized breakthrough concentration would be zero for $t < t_b$, and unity for greater values of time.

D. Breakthrough Curves for Continuous Injection

Upon substitution of Eqs. (22) and (21) into Eq. (20), the following result is obtained:

$$\xi_f(t) = 1 - \Phi\left\{\frac{\ln(t_b / t) - \sigma^2/2}{\sigma}\right\} = \Phi\left\{\frac{\ln(t / t_b) + \sigma^2/2}{\sigma}\right\} \qquad (23).$$

Finally, note that t/t_b can be replaced by a dimensionless time, τ, to obtain:

$$\xi_f(\tau) = \Phi\left\{\frac{\ln(\tau) + \sigma^2/2}{\sigma}\right\} \qquad (24).$$

Figure 1 contains a plot of normalized concentration versus dimensionless time for values of σ ranging from 0.0 to 2.5. For $\sigma = 0$, the breakthrough curve is a step function at $\tau = 1$. As σ increases, the concentration at early time, for example, at a compliance boundary, increases very rapidly, reaching almost 10% of the injected concentration when the time is only 1/1000 of the "mean" breakthrough time, for $\sigma = 2.5$.

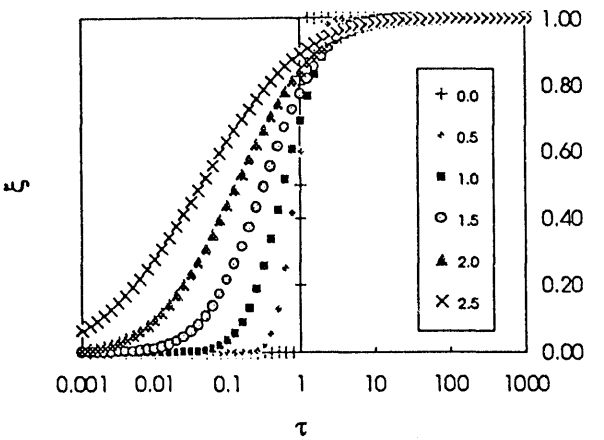

Figure 1. Normalized breakthrough curves for continuous injection. The legend gives values of σ.

By similar manipulations, the volumetric average dimensionless concentration can be obtained as a function of dimensionless time:

$$\xi_v(\tau) = \Phi\left\{\frac{\ln(\tau) - \sigma^2/2}{\sigma}\right\} \qquad (25)$$

Equation (25) differs from the flow-rate weighted average of Eq. (24) in the sign of $\sigma^2/2$. A larger value of dimensionless time is required to reach a particular value of dimensionless concentration for the volume average (*i.e.*, resident concentration) than for the flow average (*i.e.*, flux concentration). In fact, on a logarithmic plot, the curve defined by Eq. (25) can be obtained by shifting the values from Eq. (24) to the right by σ^2. Such a concentration profile might be observed experimentally by repeated logging or by tomographic imaging

E. Concentration vs. Distance Profiles

Instead of considering a fixed distance x and calculating the concentration as a function of time, we now consider a fixed time and obtain concentration profiles as functions of distance instead of breakthrough curves as functions of time. We then rearrange Eq. (21) to define the average value of x instead of the average breakthrough time:

$$\langle x \rangle \equiv \frac{t\langle u \rangle}{\langle \phi R \rangle} \qquad (26).$$

Upon inserting this expression into Eq. (19) and rearranging the result, we obtain for the volume-weighted average concentration profile:

$$\xi_v = 1 - \Phi\left\{\frac{\ln(\eta) + \sigma^2/2}{\sigma}\right\} \qquad (27),$$

where the dimensionless distance η is just $x/\langle x \rangle$. Similarly, the flow-weighted average concentration profile is

$$\xi_f = 1 - \Phi\left\{\frac{\ln(\eta) - \sigma^2/2}{\sigma}\right\} \qquad (28).$$

It is not clear that the function defined by Eq. (28) can be measured experimentally, although it can be as easily computed in simulation studies as the volume-weighted profile. It may possibly be approximated in the study of Butters *et al.*[11] by the profiles of concentration vs. depth in each sample tube cluster at each of the different times samples were taken, since sampling required drawing a finite quantity of fluid from each sample tube. This would tend to give a flux concentration rather than a resident concentration.

III. DISPERSIVITY

We note that nowhere in the preceding analysis has the concept of dispersivity been needed. In fact, it arises from the assumption that local random mixing within a porous medium behaves, statistically, the same as molecular Brownian motion. The latter leads to molecular diffusion, in which the diffusive flux is proportional to the concentration gradient of the diffusing species. If the pore-scale mixing behavior in porous solids exhibits the same statistical behavior, then it seems entirely reasonable to *assume* that the same form of differential equation should apply to describe mixing in terms of a local concentration gradient. One merely replaces the diffusion coefficient by the dispersion coefficient, which in turn is replaced by the product of the dispersivity, α, and the fluid velocity. The resulting differential equation is generally called the *convection-dispersion equation* (CDE). In order to compare the behavior of the purely advective, perfectly stratified model based on the log-normal distribution with the classical approach, we now review some solutions of the CDE.

A. Solutions of the Convection-Dispersion Equation

Arya *et al.*[2] presented the following solution to the one-dimensional CDE for a system of fixed length L:

$$\xi(t_D, x_D) = \frac{1}{2}\operatorname{erfc}\left[\frac{x_D - t_D}{2\sqrt{t_D/Pe}}\right] + \frac{1}{2}\exp(x_D Pe)\operatorname{erfc}\left[\frac{x_D + t_D}{2\sqrt{t_D/Pe}}\right] \qquad (29)$$

The dimensionless quantities in Eq. (29) are defined by

$$x_D \equiv \frac{x}{L} \qquad t_D \equiv \frac{vt}{L} \qquad Pe \equiv \frac{L}{\alpha} \qquad (30),$$

where the dispersivity, α, is assumed to be a constant characteristic of the porous medium in the derivation of Eq. (29), and Pe is the Peclet number, a measure of the relative importance of advection and dispersion. A large value of Pe implies a relatively sharp displacement front, and a small value corresponds to a broad mixing zone.

B. CDE Breakthrough Curves

In order to obtain a breakthrough curve, we merely substitute unity for the dimensionless distance in Eq. (29) and note that L/v is a measure of average travel time for a contaminant moving with the fluid. A retardation coefficient can be easily introduced to obtain a definition of dimensionless time similar to the one used for the log-normal model. If, in addition, we replace the complementary error functions, by using the identity

$$\frac{1}{2}\operatorname{erfc}(u) = \Phi\left(-\sqrt{2}u\right) \qquad (31),$$

we obtain, after some manipulation

$$\xi_{cx}(\tau) = \Phi\left\{\sqrt{\frac{Pe}{2}}\left(\tau^{1/2} - \tau^{-1/2}\right)\right\} + \exp(Pe)\Phi\left\{\sqrt{\frac{Pe}{2}}\left(\tau^{1/2} + \tau^{-1/2}\right)\right\} \qquad (32).$$

The use of the normal probability integral instead of the complementary error function provides a slight

computational advantage when using some software packages.

C. CDE Concentration Profiles

Similarly, we can obtain the concentration profile equation from Eq. (29), but we consider a fixed time t, define x_m by $x_m = vt$, and assume that $x_m << L$. After some manipulation, we obtain

$$\xi_{CD}(x/x_m) = \Phi\left\{\sqrt{\frac{Pe'}{2}}(1-x/x_m)\right\} + \exp\left(\frac{x}{x_m}Pe'\right)\Phi\left\{\sqrt{\frac{Pe'}{2}}(1+x/x_m)\right\} \quad (33)$$

The explicit form x/x_m is retained in Eq. (33) instead of introducing a dimensionless distance in order to distinguish the argument of the equation from the one used in the log-normal model. Note also that the Peclet number is now defined using x_m for the characteristic length instead of L.

D. Displacement Scaling

Hewett and Behrens[4] modeled displacements in two-dimensional vertical systems with a fairly large number of grid blocks to illustrate the effect of heterogeneity in the permeability distribution on dispersive behavior. For miscible displacement in a *homogeneous* system, the concentration profile as a function of distance from the inlet scales according to classical dispersion theory, with a mixing zone width proportional to the square root of the median distance traveled by the displacement front, and a constant dispersion coefficient which can be calculated from the grid block and time step sizes.

The normalized concentration as a function of distance traveled is given approximately by

$$\xi_{CD}(x/x_m) = \frac{1}{2}\operatorname{erfc}\left[\frac{1}{2}\left(\sqrt{\frac{x_m}{\alpha}}\left\{\frac{x}{x_m}-1\right\}\right)\right] \quad (34).$$

Equation (34) will be recognized as being mathematically identical to the first term of Eq. (29). The neglect of the second term is valid for Pe greater than about 10.

The mixing zone width is defined[4] as the difference between $x_{0.1}$, where ξ_{CD} is 0.1, and $x_{0.9}$, where ξ_{CD} is 0.9. Solving Eq. (34) for these two values of x yields, approximately,

$$W_{CD} = 3.624775\sqrt{x_m}\sqrt{\alpha} \quad (35).$$

This may be compared with the in-situ concentration profile calculated from the log-normal model. For this purpose, we write Eq. (27) for the desired values of ξ:

$$p = 1-\Phi\left\{\frac{\ln(x/\langle x\rangle)+\sigma^2/2}{\sigma}\right\} \quad (36),$$

and solve for $x_{0.9}$ and $x_{0.1}$, corresponding to p = 0.9 and 0.1, respectively. Then the width of the mixing zone for the log-normal model is

$$W_{LN} = 2\langle x\rangle\exp\left(\frac{-\sigma^2}{2}\right)\sinh(1.281552\sigma) \quad (37).$$

By setting the two expressions [Eqs. (35) and (37)] for mixing zone width equal to each other, we can determine a value for effective dispersivity for fitting the classical dispersion equation to the log-normal model. However, there is one ambiguity, *viz.*, the correspondence between the mean, $\langle x\rangle$, and x_m. Since the latter is often described as the mean distance traveled, it is tempting to set them equal. However, this leads to a definition of dispersivity which is not a monotonic function of σ. This merely reflects the fact that, as σ increases, the convection-dispersion solution cannot be made to resemble the log-normal function at all well, at least in the spatial domain.

In fact, there are many different methods given in the literature for calculating a Peclet number, or, equivalently, an effective dispersivity, from different computed characteristics of measured breakthrough curves in tracer experiments or from detailed model calculations. None of them is entirely satisfactory, as will become apparent in the following discussion.

Neretnieks, Eriksen, and Tähtinen[15] considered this problem for analyzing their measured breakthrough curves for tracers flowing through a single fracture, and used an expression mathematically equivalent to Eq. (32) to calculate an effective Peclet number. Since they were working with concentration vs. time rather than concentration vs. distance, they defined a normalized mixing zone size as

$$\omega_{CD} = \frac{t_{0.9}-t_{0.1}}{t_{0.5}} \quad (38)$$

and used a graph of Pe vs. ω_{CD} to calculate an effective Pe from measured values of the times in Eq. (38). Hence, they used the median value in their analysis, but one should keep in mind that they worked with breakthrough curves (concentration vs. time) instead of concentration vs. distance profiles.

The distance domain should, in principle, be entirely equivalent to the time domain, and, using $Pe = x_m/\alpha$ in Eq. (35), we find:

$$Pe = \left(\frac{3.624775}{W_{cd} / x_m} \right)^2 \qquad (39)$$

A plot of this function (not shown here) agrees closely with the diagram given by Neretnieks et al.[15] for the Peclet number as a function of the normalized mixing zone duration, at least for Peclet numbers greater than about 5. For the time being, we will use the median for calculating an effective dispersivity.

Noting that the coefficient of the hyperbolic sine term in Eq. (37) is just twice the median of x, setting the two expressions for mixing zone width equal to each other, and solving for α results in

$$\alpha = 0.304437[\sinh(1.28155\sigma)]^2 x_{0.5} \qquad (40)$$

Equation (40) shows that the assumption of log-normality leads to an effective dispersivity which increases linearly with the median distance traveled. Another way of stating this behavior is to note that it is equivalent to a Peclet number which does not change with distance. Furthermore, the coefficient of distance, *i.e.*, the inverse Peclet number, increases exponentially with σ. Figure 2 is a plot of dispersivity [calculated from Eq. (40)] versus distance, for a range of values of σ.

Also shown in Fig. 2 are experimental values, transferred from a plot given by Arya *et al*,[2] at a very broad range of scales. The "Lab" points were originally compiled by Arya,[16] those labeled "P-G" are from Pickens and Grisak,[17] and those labeled "L-B" are from a compilation by Lallemand-Barrès and Peaudecerf.[18]

The comparison between the log-normal model and the experimental data is interesting for several reasons. First, by choosing an appropriate range of values of σ, the entire region of experimental points can be swept. Second, it seems likely that the data were extracted from systems with very different permeability distributions, and that analyzing of the experiments in terms of the log-normal model instead of the convection-dispersion model might possibly remove much of the apparent scatter.

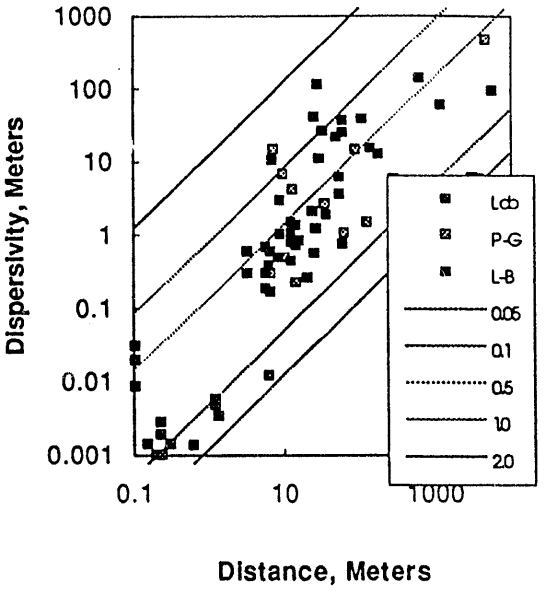

Figure 2. Plot of effective dispersivity, α, versus median distance traveled. The lines are calculated from the log-normal model for σ ranging from 0.05 for the lowest line to 2.0 for the upper. Points are experimental values from sources given in the text.

Also, there is quite a bit of ambiguity in determining the Peclet number from observed breakthrough or profile curves, especially when the effective dispersivity is large. As shown below, the use of different characteristics of the curves to calculate Peclet numbers can give very different answers when the mixing zone is large.

Finally, the plot suggests that a value of less than about 2 for σ may be a good guess in the absence of field data at the scale of interest. However, this may be biased toward low values because many of the field observations were made in porous media rather than in fractured rock, and it is generally believed that fractured media have more heterogeneous permeability distributions than do porous media.

E. Model Displacements in Heterogeneous Systems

To study the effect of permeability heterogeneity, Hewett and Behrens[4] also modeled displacements in

which the permeability in a 200 (horizontal) by 20 (vertical) grid was assigned by a random fractal process, so that permeabilities are spatially correlated at all length scales. They then calculated effective mixing lengths and dispersion coefficients by using the 0.1 and 0.9 fractiles on the concentration vs. distance profiles, as outlined above in discussing the log-normal model.[a] A log-log plot of their results as functions of distance has slopes of 0.991 and 0.982 for the mixing length and dispersion coefficient, respectively. This is obviously in much closer agreement with the log-normal model than with the classical theory.

IV. BREAKTHROUGH AND PROFILE CURVES FOR THE TWO MODELS

It should be noted that, while it is possible to fit log-normal *breakthrough* curves quite well with a convection-dispersion solution for almost any value of σ, the shapes of the two functions are quite different when *profile* curves are compared for even moderately large values of σ. This is illustrated in Figures 3 and 4.

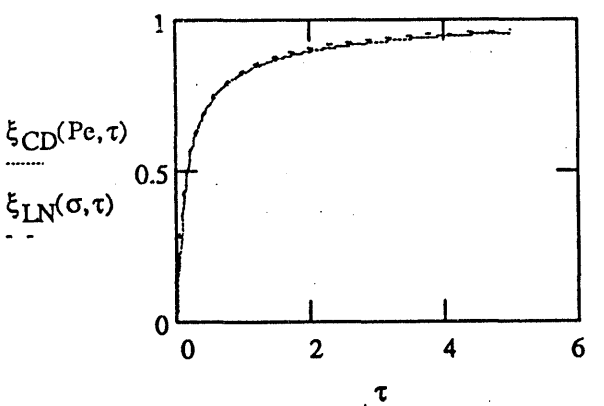

Figure 3. Comparison of log-normal and convection-dispersion breakthrough curves with σ = 1.9 and Pe = 0.2, respectively.

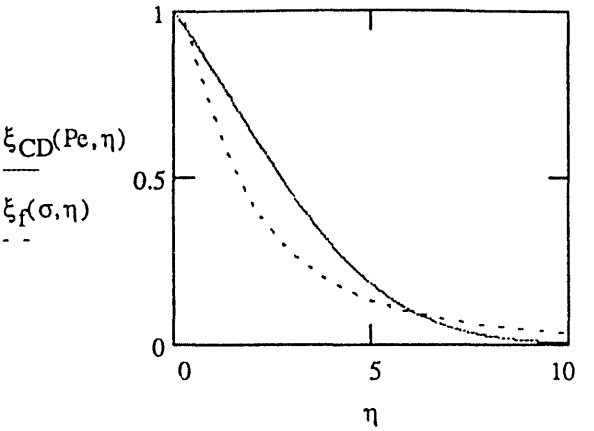

Figure 4. Comparison of log-normal and convection-dispersion concentration versus distance profiles, with σ = 1.0 and Pe = 0.2, respectively.

A. Matching Breakthrough Curves

In constructing Fig. 3, the Peclet number was assigned, and Eq. (32) was used to find the 0.1, 0.5, and 0.9 fractiles of the breakthrough curve, by assigning p = 0.1, 0.5, and 0.9, respectively, in

$$p = \Phi\left\{\sqrt{\frac{Pe}{2}}\left(\tau^{1/2} - \tau^{-1/2}\right)\right\} + \exp(Pe)\,\Phi\left\{\sqrt{\frac{Pe}{2}}\left(\tau^{1/2} + \tau^{-1/2}\right)\right\} \qquad (41).$$

Equation (41) is mathematically equivalent to the solution to the CDE given by Neretnieks *et al.*[15] Then the following equation was solved for σ:

$$2\sinh(1.281552\sigma) = \frac{\tau_{.9} - \tau_{.1}}{\tau_{.5}} \qquad (42)$$

As shown in Fig. 3, the log-normal and CDE breakthrough curves are almost indistinguishable, although the individual fractiles do not match exactly.

Since the two expressions produce very nearly the same breakthrough curves for appropriate choices of the parameters, they will fit experimental *breakthrough* data equally well. In fact, as noted by Moreno *et al.*,[19] it is not possible to discriminate between dispersion models and channeling models at a fixed migration distance, even by using a number of different tracers with differing retardation coefficients.

[a] We note that the profiles are easy to work with in simulation studies, since a number of profiles can be obtained at a series of time values from a single simulation run. However, experimentally, it is much easier to work with breakthrough curves.

B. Matching Profile Curves

In contrast, the profile curves shown in Fig. 4 do not agree at all. The curve shown for the log-normal model corresponds to the flow-weighted average, since the resident concentration curve does not even cross the CDE solution, except near the origin, for Pe less than 1.

In constructing Fig. 4, Eqs. (33), (27), and (28) were solved for the 0.1, 0.5, and 0.9 fractiles for the CDE, volume-weighted log-normal, and flow-weighted log-normal profiles, respectively. For values of $\sigma \leq 0.2$ (approximately), a value of Pe can be chosen by matching the dimensionless widths to obtain reasonably close agreement among the profile curves.

However, for larger values of σ, not even an approximate match could be obtained by this method. Accordingly, we matched the actual width by solving

$$\left(\frac{x}{x_m}\right)_{.1} - \left(\frac{x}{x_m}\right)_{.9} = 2\sinh(1.281552\sigma)\exp(\sigma^2/2) \quad (43),$$

where the LHS is obtained from the CD equation and the RHS by solving the flow-averaged concentration, given by Eq. (28), for the appropriate fractiles.

Although Eq. (43) has a solution for Pe = 0.2, Fig. 4 shows that the CD and LN profile curves not only have different shapes, the resulting value of σ for a "match" is about 1.0, compared to 1.9 from fitting the breakthrough curves for the same Peclet number.

C. Distance Re-scaling

This problem arises because, for the small values of *Pe* required to give a broad mixing zone, the mean travel distance of the tracer or contaminant is not equal to x_m, as assumed in the derivation of the solution to the one-dimensional CD equation given by Eq. (33). The actual dimensionless mean distance traveled can be obtained from the integral

$$\frac{\langle x \rangle}{x_m} \equiv \gamma = \int_0^\infty \xi_{cd}(\chi; Pe)\, d\chi \quad (44),$$

where $\chi = x/x_m$, and the integrand is given by Eq. (33).

Note that γ is a function of *Pe*. Numerical evaluation of Eq. (44) results in the plot shown in Fig. 5, which shows that γ approaches unity for large values of *Pe*, and does not depart significantly from unity until *Pe* is less than about 10. Unfortunately, it is precisely this range of Pe values that is required to match field-scale transport experiments with the CD model.

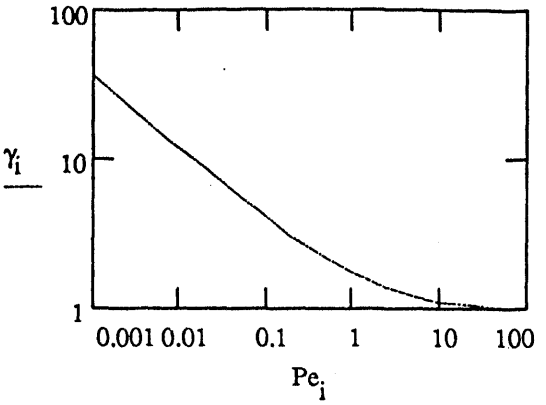

Figure 5. Dimensionless mean distance traveled for the one-dimensional convection-dispersion equation solution as a function of Peclet number.

Clearly, this shift in the mean distance traveled must be taken into account in attempting to match the CD solution to the log-normal model. The following procedure is used:

1. For a given value of *Pe*, calculate γ by numerical integration of Eq. (44).
2. Calculate $\eta_p = (x/x_m)_p$ for $p = 0.1$, 0.5, and 0.9, by numerical solution of Eq. (33).
3. Calculate $(\eta_{.1} - \eta_{.9})/\eta_{.5}$. This normalized width remains constant when all distances are re-normalized, using $\langle x \rangle$ instead of x_m.
4. Set the resulting ratio equal to $2\sinh(1.281552\sigma)$ and solve for σ.
5. For plotting, change the argument of the CD solution to $\gamma\eta$, where η is the argument of the LN model.

The net result of this sequence of operations is to match the mean distance traveled as well as the normalized width of the two models. An example application is shown in Fig. 6, with Pe = 0.2, $\gamma = 3.065$, and $\sigma = 0.689$, using the volume-average normalized concentration for the log-normal model. The agreement between the two curves is now quite good.

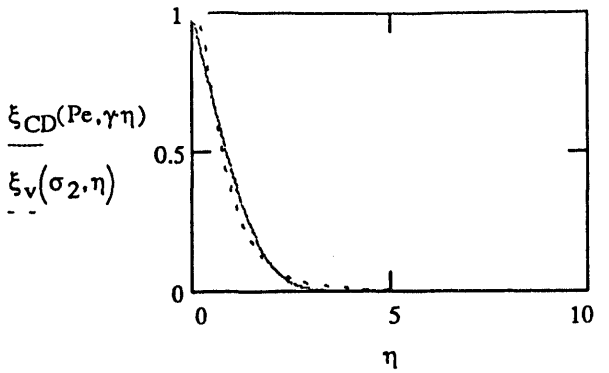

Figure 6. Normalized concentration profiles from the one-dimensional convection-dispersion equation and the log-normal model, with Pe = 0.2 and σ = 0.689, respectively. The distance for the CD solution is re-scaled by the factor γ = 3.065.

Although the two curves now match rather closely, note that, with a given small Peclet number, the σ value from the breakthrough curve (1.9) is very different from the value obtained by matching the flow profile. Conversely, if we consider the log-normal curves to represent at least approximately the behavior of field-scale transport processes, then we would calculate very different values of the Peclet number for the same value of σ. Hence, there is little predictive utility in the convection-dispersion approach to analyzing field-scale transport, since the results have to be re-scaled for each time or distance of interest.

All of this tinkering is made necessary by attempting to replace a heterogeneous system by an "equivalent" homogeneous medium, characterized by an average permeability, in which the apparent mixing scale can be represented by an appropriate choice of the dispersivity. The concept of an equivalent homogeneous medium is tied closely to the concept of a representative elemental volume, which may not exist, or, if it does, almost certainly is not the same for flow as for transport.

Matheron and de Marsily[3] showed that an equivalent homogeneous medium can exist only if the transport system is large enough to reach an asymptotic limit of Fickian (*i.e.*, dispersive) behavior. Physically, this requires a mechanism for transverse advective mixing. In media which are even partially stratified (or, equivalently, in which either independent or at most weakly interacting "channels" exist), the time and distance scales required for this limit to be reached may be so large that gross alterations in the geologic framework, such as faults or facies changes, are encountered first.

V. PECLET NUMBERS AND CURVE CHARACTERISTICS

In attempting to force field data to fit the convection-dispersion theory, many investigators have derived relationships between the Peclet number and various characteristics of breakthrough curves and concentration profiles, based on analytical or numerical properties of Eq. (29), or of approximations to this equation. For example, we previously used an approximation, Eq. (34), to derive Eq. (35) for the mixing zone width. From this equation one can derive

$$Pe = \left(\frac{3.624775 x_m}{x_{.1} - x_{.9}} \right)^2 \qquad (45).$$

There is another relationship in the form of a graph of Pe versus the normalized breakthrough duration, ω_{CD}, given by Neretnieks, et al.[15] As mentioned earlier, the graph and a plot of Eq. (45) agree closely when the Peclet number is greater than about 10.

In fact, most of the expressions for the Peclet number give similar results, when applied to the log-normal distribution, for Pe > 10, and are not too dissimilar when Pe is between 1 and 10, provided that one considers only the spatial domain (profiles) or the temporal domain (breakthrough curves). As shown above, difficulties arise when comparing both types of curves, in that different corresponding values of Pe and σ are obtained.

A. Peclet Number and Moments

A number of relationships have been reported in the literature between the Peclet number and various moments of the breakthrough curve. One of the simplest was given by Neretnieks,[10] who credited Levenspiel.[20] We define the moments of the breakthrough curve by:

$$m_p = \int_0^\infty \tau^p \left(\frac{\partial \xi}{\partial \tau} \right) d\tau \qquad (46).$$

Then, according to Levenspiel, the Peclet number can be calculated from

$$Pe = \frac{2m_1^2}{m_2 - m_1^2} \equiv \frac{2}{(CV)^2} \qquad (47),$$

where *CV* is the coefficient of variation, i.e., the ratio of the standard deviation to the mean of the breakthrough curve. This result shows clearly that the Peclet number must decrease rapidly as the breakthrough curve becomes more diffuse.

Moreno and Tsang[21] quoted the following relationships attributed to Robinson:[22]

$$Pe = \frac{1}{\sqrt{m_1 m_{-1}} - 1} \tag{48}$$

$$Pe = \frac{\sqrt{3m_2 - 2m_1^2} - 4m_1}{\sqrt{3m_2 - 2m_1^2} - m_1} \tag{49}$$

$$Pe = -\frac{\sqrt{3m_{-2} - 2m_{-1}^2} - 4m_{-1}}{\sqrt{3m_{-2} - 2m_{-1}^2} - m_{-1}} \tag{50}$$

All of these relationships between *Pe* and the moments of the breakthrough curve are based on the solution to the one-dimensional convection-dispersion equation, which is intimately related to the normal distribution. It is therefore not surprising that different results will be obtained in applying them to other distributions, such as the log-normal.

B. Moments of the Log-Normal Model

The various moments required in Eqs. (47) through (50) are easily evaluated analytically for a log-normal breakthrough curve. The following equation is valid for all real values of *p*:

$$\langle m_p \rangle = e^{p\langle \ln t \rangle} e^{p^2\sigma^2/2} \tag{51}.$$

Then, upon using Eq. (51) for the different moments required and substituting the results into Eqs. (47) through (50), we obtain the following expressions for *Pe* as a function of σ:

$$Pe = \frac{2}{e^{\sigma^2} - 1} \tag{52}$$

$$Pe = \frac{1}{e^{\sigma^2/2} - 1} \tag{53}$$

$$Pe = \frac{\sqrt{3e^{\sigma^2} - 2} - 4}{\sqrt{3e^{\sigma^2} - 2} - 1} \tag{54}$$

$$Pe = -\frac{\sqrt{3e^{\sigma^2} - 2} - 4}{\sqrt{3e^{\sigma^2} - 2} - 1} \tag{55}.$$

Equations (52) and (53) give similar results for small values of σ, in that *Pe* approaches $2/\sigma^2$ as $\sigma \to 0$. Also, for large values of σ, *Pe* tends to zero for both expressions. The Peclet number calculated from Eq. (54) approaches $-2/\sigma^2$ as $\sigma \to 0$, and +1 as $\sigma \to \infty$, while the value calculated from Eq. (55) approaches $+2/\sigma^2$ as $\sigma \to 0$ and -1 as $\sigma \to \infty$. Hence, the latter two equations give physically meaningless results for some values of σ, and neither of them seems to work for values of *Pe* much less than one. Once again, this reflects the difficulty of fitting log-normal behavior — and presumably real transport data in heterogeneous systems — by using the CDE solution with small constant values of the Peclet number.

VI. PULSE RELEASE

Of more interest than the solution for continuous release of a tracer or contaminant is the case of a finite pulse, from which one can easily develop the breakthrough curve for an arbitrary but given time-dependent release function by convolution. Consider a release starting at time 0, with concentration remaining constant until the release stops at time Δt. We can immediately write, from Eq. (24),

$$\xi = \Phi\left\{\frac{\ln(\tau) + \sigma^2/2}{\sigma}\right\} - \Phi\left\{\frac{\ln(\tau - \delta) + \sigma^2/2}{\sigma}\right\} \tag{56},$$

where $\delta = \Delta t / t_b$ is the dimensionless pulse duration. When τ is less than δ, only the first term of Eq. (56) is used. Figure 7 is a plot of the pulse breakthrough curves for a range of values of σ, with δ held constant at 0.001.

The effect of increasing σ is somewhat surprising. For small values of σ, the breakthrough peak is nearly symmetric and occurs near $\tau = 1$. The shape is essentially Gaussian, so there would be little if any observable difference between a log-normal breakthrough curve and a convection-dispersion breakthrough curve for a tracer pulse test.

As σ increases, the breakthrough curve broadens and the peak concentration at first decreases, which could be interpreted as greater dilution. However, the location of the maximum shifts toward earlier time, so that more contaminant is produced early. Also, a long right tail develops, as shown for $\sigma = 0.5$ in Fig. 7. The shape of the

central part of the curve is still nearly Gaussian, and a fit with a convection-dispersion solution would be a reasonable approximation, especially if matrix diffusion is included.[15]

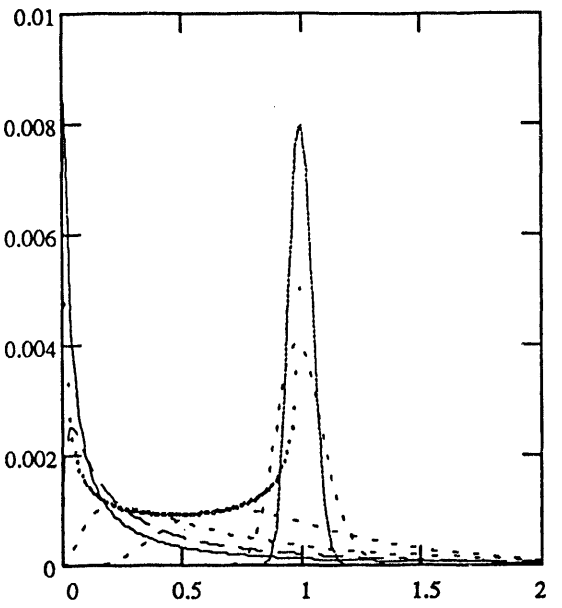

Figure 7. Pulse breakthrough curves for δ = 0.001 and σ values of 0.05, 0.10, 0.50, 1.00, 1.50, and 2.00, reading from the sharp peak on the right to the sharp peak on the left, respectively. The "U" shaped curve is the locus of the maxima in the breakthrough curves.

However, with further increases in σ, the shift of the peak toward earlier time continues, and its magnitude begins to *increase* rapidly. Now the departure from a Gaussian shape is pronounced, and no amount of tinkering with the convection-dispersion approach will provide an adequate representation of the breakthrough curve. This is exactly the sort of behavior intuitively associated with the existence of "fast pathways" in a flow and transport system, in which only limited dilution occurs.

The behavior of the peak concentration as a function of σ can be derived analytically from Eq. (56) for small values of δ. First, this equation is differentiated with respect to τ. The result is then expanded as a Taylor's series through second order in δ, and equated to zero to find the location of the maximum, τ_{max}. The result, after considerable manipulation, can be reduced to

$$\tau_{max} = \exp\left(-\frac{3}{2}\sigma^2\right)\left[1+\frac{\delta}{2e^{-3\sigma^2/2}+\delta}\right] \qquad (57).$$

The size of the peak is then obtained by substituting the RHS of Eq. (57) into Eq. (56) and again expanding in a second-order Taylor's series in δ. The result is

$$\xi_{max} = \frac{\delta}{\sigma\sqrt{2\pi}}\exp(\sigma^2) \qquad (58).$$

Eqs. (57) and (58) were used to calculate corresponding values of the peak height and the times at which they occur for plotting the locus of the peak in Fig. 7. The peak height tends toward infinity as $1/\sigma$ for small σ and exponentially as σ^2 for large σ.

It is of particular interest that the peak height predicted by Eq. (58) is proportional to the pulse duration. By differentiating this expression with respect to σ, equating the result to zero, and solving for σ, we can find the value for which the peak height is a minimum:

$$\sigma_{min} = \frac{\sqrt{2}}{2} \approx 0.707 \qquad (59).$$

The minimum peak height is then

$$(\xi_{max})_{min} = \frac{\delta}{\sqrt{\pi}}\exp\left(\frac{1}{2}\right) \approx 0.930\cdot\delta \qquad (60),$$

and it occurs at dimensionless time

$$\tau_{min} = \exp\left(-\frac{3}{4}\right) \approx 0.472 \qquad (61).$$

Equation (60) shows that the peak breakthrough concentration can never be less than about one times the dimensionless pulse duration. In other words, *there is a limit to the reduction of effluent contaminant concentration by dilution.*

It should be noted that this analysis is valid only for values of σ such that the peak occurs later than $\tau = \delta$. Otherwise, the maximum is determined by using only the first term of Eq. (56), evaluated at $\tau = \delta$. By setting the LHS of Eq. (57) equal to δ and solving for σ, we find that

$$\sigma_{max} = \sqrt{-\frac{2}{3}\ln\left(\frac{\delta}{2}\right)} \qquad (62),$$

which gives a value of 2.25 for the maximum value of σ when $\delta = 0.001$. In the limit of an infinitesimal pulse, the analysis remains valid as σ increases without limit.

A. Cumulative Contaminant Production

As a result of the shift of the peak toward early time and its increasing magnitude with larger σ, more of the total contaminant mass released in the pulse is produced early. The normalized cumulative contaminant mass production, $\Xi(\tau,\delta,\sigma)$, is easily obtained by integrating Eq. (56) over the dimensionless time:

$$\delta \cdot \Xi(\tau,\delta,\sigma) = \tau\Phi\left(\frac{\ln\tau + \frac{\sigma^2}{2}}{\sigma}\right) - \Phi\left(\frac{\ln\tau - \frac{\sigma^2}{2}}{\sigma}\right) + \Phi\left(\frac{\ln(\tau-\delta) - \frac{\sigma^2}{2}}{\sigma}\right) - (\tau-\delta)\Phi\left(\frac{\ln(\tau-\delta) + \frac{\sigma^2}{2}}{\sigma}\right) \quad (63)$$

In Eq. (63), the terms including $(\tau-\delta)$ are set identically to zero for all $\tau < \delta$. Figure 8 shows a plot of the normalized cumulative contaminant produced as a function of dimensionless time, for $\delta = 0.001$. As τ tends toward infinity, the normalized production approaches unity in all cases.

Figure 8 shows that the fraction of the contaminant pulse produced at early time increases very rapidly as σ increases, again coinciding with intuitive notions of transport along fast paths. From Eq. (63), it can be shown that, in the limit $\delta = 0$, the cumulative fraction of injected contaminant mass produced is given by:

$$\lim_{\delta\to 0}\{\Xi(\tau,\delta,\sigma)\} = \Phi\left\{\frac{\ln\tau + \sigma^2/2}{\sigma}\right\} \quad (64).$$

Eq. (64) shows that a plot of the cumulative fraction of injected mass produced, on a normal probability scale, vs. time, on a logarithmic scale, will produce a straight line, when the pulse width is very small compared to the mean breakthrough time. It is also obvious that the dimensionless time required to produce 50% of the injected mass is given by:

$$\tau_{0.5} = \exp(-\sigma^2/2) \quad (65)$$

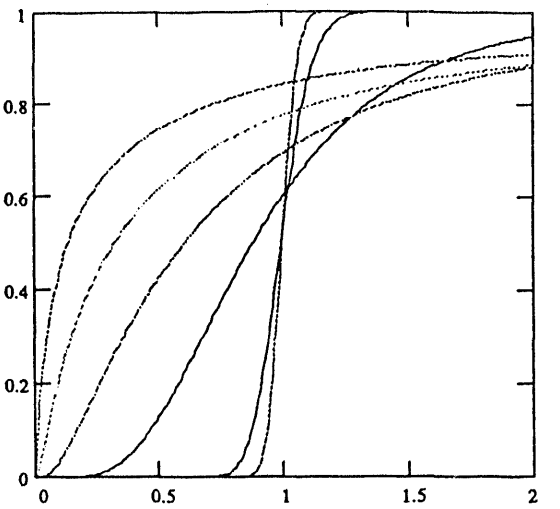

Figure 8. Normalized cumulative contaminant production versus dimensionless time for the same range of σ values as in Fig. 7. For all 6 curves, $\delta = 0.001$

VII. DISCUSSION

In deriving the form of the log-normal model presented here, we started with the idea of completely independent strata in a linear flow system, assumed that the permeabilities of these layers formed a log-normal distribution, then passed to the limit of a continuum to obtain the closed forms in terms of the normal probability function. In principle, the σ parameter is to be obtained from permeability measurements on cores.

A. Waterflooding Applications

In the author's experience, this determination of σ from core data works quite well when there are many permeability measurements, the system is moderately heterogeneous, and there is essentially no fracture permeability,[6] which of course is not sampled on a meaningful scale by coring. However, it was also found that adjusting σ, in the case of waterflooding oil reservoirs, for pattern effects (i.e., non-linear and variable-length flow paths), mobility ratios, variable porosity and oil saturation, *etc.*, improves the match of predicted waterflood response to actual results, compared to simply using the value of σ from core permeability measurements. These adjustments were derived from various literature sources, by fitting the log-normal model to breakthrough curves.

If the flow response — either from field projects or from detailed, highly resolved simulations — is used to determine σ, the match between observed and calculated response is, of course, improved. What is interesting is that the log-normal functional form is closely followed by real displacement experiments and detailed simulations, and that often only minor adjustments in parameter values are required to match field data or simulator output with simple analytic expressions.

For example, this approach completely ignores capillary imbibition in waterflooding, which can contribute significantly to the overall recovery efficiency. The displacement front in the more permeable strata will tend to move ahead of the front in less permeable intervals. This will create regions of relatively high *water* saturation adjacent to regions of relatively high *oil* saturation. Water will then imbibe into the low-permeability region, displacing oil into the adjacent high-permeability interval where it can be swept to the producing well. In an unpublished study, it was found, by simulating displacement in a symmetry element from a five-spot pattern containing 10 log-normally distributed layers, that including the effects of capillarity reduced the effective value of σ by a few percent from the value used to generate the layer permeabilities.

This experience and others over the past twenty or so years have led the author to suspect that displacement processes in heterogeneous materials are fundamentally log-normal, or very nearly so. The speculation is that the functional forms, given by Eqs. (23), (24), (27), and (28), are capable of realistically modeling breakthrough and concentration profile curves even when the underlying distribution is not particularly close to log-normal, the system is not really stratified, and the elements strongly interact with each other.

B. Transport in the Soil Vadose Zone

This notion is reinforced by the experiment of Butters an co-workers.[11,12] Even though the flow direction was essentially perpendicular to the stratification of the soil, the movement of the tracer pulse was much better represented by a log-normal model than by the solution to the CDE. They found that fitting the CDE solution at a given depth did not result in a good prediction even for the next depth, only 30 cm below. For most of the depths sampled, the value of σ derived from the CV was between 0.4 and 0.5, which is smaller than the waterflood example (about 0.7) reported by Chesnut[9] and very much smaller than the value of about 1.7 obtained by fitting the data[8] for the groundwater flow distribution measured by others in the Stripa experiment.

By calculating the moments of individual breakthrough curves, Butters *et al.*[12] computed averages and variances for each individual square in their pattern, and reported the averages of these values as "local scale" averages. Assuming log-normality, the average value of σ calculated from these data is about 0.38. In addition, they averaged the concentrations at each depth at each time to produce a field average breakthrough curve at each depth. Again assuming log-normality, the reported means and variances were used to calculate σ for each depth; the average of these values is about 0.49.

Finally, they also reported results[11] of measuring the saturated hydraulic conductivities of 56 randomly selected surface samples of soil in the plot. The CV of these measurements was reported to be 0.44, which corresponds to a value of σ equal to 0.42. The agreement with transport-derived values may be fortuitous, but it fits with the author's success in using core analysis data to obtain a close estimate of σ for the Benton waterflood.

C. Strongly Heterogeneous Systems

The behavior of the breakthrough curve for pulse injection shown in Fig. 7 is remarkably similar to behavior reported by Moreno and Tsang[21] in their study of strongly heterogeneous systems. They simulated steady-state flow and transport (by particle tracking) in a number of realizations of a 20x20x20 cube (some runs were made for a 40x40x40 gridblock model), with permeability values assigned according to a log-normal distribution and an exponential correlation function. The correlation length was generally $0.1L$, where L is the side of the cube, but some runs were made with $0.05L$ and $0.20L$. The mean of the distribution was adjusted to maintain constant total flow through the cube, and calculations were made for σ equal to 0.10, 0.20, 0.50, 2.00, 4.00, and 6.00.

The breakthrough curves, as σ varies, show exactly the same qualitative behavior depicted in Fig. 7, with a sharp, symmetric peak at $\tau = 1$ for $\sigma = 0.10$. The peak is progressively broader, but remains relatively symmetrical and located near $\tau = 1$, for $\sigma = 0.20$ and 0.50. For $\sigma = 2.00$, the breakthrough curve becomes very diffuse, with a broad, low peak of indeterminate location. Its location is definitely at a value of τ much less than 1, probably between 0.2 and 0.6. Finally, for $\sigma = 4.00$, a high, sharp peak develops near $\tau = 0.1$. It becomes even sharper and moves further to the left when $\sigma = 6.00$. This development of a short travel time for the peak concentration to reach

the outflow boundary was termed the "fast channeling effect." In both of the latter two cases, the breakthrough curve also develops a long right tail.

Moreno and Tsang also showed traces of the flow paths through the cube from the inlet face to the outflow face on the opposite side, for channels that provided most of the flow. For $\sigma = 1.00$, there are many channels, fairly uniformly distributed across the inflow face and running reasonably straight to the outflow face. They do not appear to interact significantly, although interaction is not excluded by the code used or by the properties inserted into the model.

The behavior is very different for $\sigma \geq 4.00$. Based on the one realization shown in their paper, and the authors' description of others, the channels coalesce into a few (two or three) coherent bundles, each spanning a few grid blocks in the direction transverse to the principal flow direction. They are more convoluted in the longitudinal direction than the channels for smaller σ, but still reasonably straight. This flow geometry is consistent with our intuitive ideas of flow paths within fractured rock, and yet *it develops in a stochastic porous medium model, without any explicit representation of fractures.*

As shown in Fig. 7, the simple analytic expressions obtained from the log-normal model reproduce the breakthrough behavior observed by Moreno and Tsang. The only difference is that their breakthrough curves are much less sensitive to σ than the analytical expressions are. This reduced sensitivity is due to the fact that, as σ increases, flow is confined to a smaller and smaller number of channels. By constructing histograms of the permeability distribution along the channels responsible for 90% of the flow, Moreno and Tsang found that the peak of the flow distribution is shifted to a higher permeability, and its logarithmic variance reduced, relative to the input or "global" distribution used to construct the realization. If we denote the natural log standard deviation of the input distribution by $\sigma_{\ln k}$, then the "effective" σ for transport, σ_t, is less than $\sigma_{\ln k}$.

It is of considerable interest to explore the relationship between these parameters. Moreno and Tsang reported values for the Peclet number calculated from the moments of the breakthrough curves, using Eqs. (48) through (50). We then used the relationships between σ and *Pe* given by Eqs. (53) through (55) to estimate values for σ_t. Table I summarizes the results obtained from Eq. (53). Essentially the same values were obtained from the other two equations for $\sigma_{\ln k} \leq 2.00$. For the remaining cases, there were significant differences among the different estimates of *Pe*, and, consequently, the corresponding estimates of σ_t. However, as the authors stated, dispersion cannot be described by the advection-dispersion equation for strongly channeled flow, and this is reflected in the variation of Pe calculated from different features of breakthrough curves.

Table I. Values of the effective transport heterogeneity parameter, σ_t, estimated from Eq. (53) and Peclet numbers reported by Moreno and Tsang.[21]

$\sigma_{\ln k}$	*Pe*	σ_t	$\sigma_t/\sigma_{\ln k}$
0.10	2076	0.031	0.310
0.20	522	0.062	0.309
0.50	84	0.154	0.308
1.00	21	0.305	0.305
2.00	5.8	0.564	0.282
4.00	1.9	0.920	0.230
6.00	0.9	1.222	0.204

As shown in Table I, the ratio $\sigma_t/\sigma_{\ln k}$ is almost constant for $\sigma_{\ln k} \leq 2.00$, and then begins to decrease. It is not clear whether this decrease is real or a numerical artifact arising from the small number of flow channels that develop in the simulations with the two higher values of $\sigma_{\ln k}$. It seems likely that the sample size may be too small to accurately define the behavior when the channeling is extreme.

In Fig. 7, the ratio of peak height at $\sigma = 0.05$ to the minimum peak height is roughly 8, as is the ratio for $\sigma = 2.00$. It is perhaps significant that about the same ratios are shown by Moreno and Tsang with $\sigma_{\ln k} = 0.10$ and 6.00, respectively. If we assume that σ_t can be estimated as $0.31\sigma_{\ln k}$, we should compare the numerical model breakthrough curves to the analytical curves with $\sigma = 0.03$ and $\sigma = 1.86$, instead of 0.10 and 6.00, which gives essentially quantitative agreement.

Some additional insight into the relationship between the permeability distribution and the flow distribution can be gained from the work of Tompson and Gelhar.[23] These numerical experiments were performed on a 51x51x51-node cube, with a log-normal permeability distribution and an exponential variogram with a correlation length equal to 0.04 times the side of the cube. They reported the average longitudinal velocity and its standard deviation for steady-state flow experiments in which $\sigma_{\ln k} = 1.0$, 1.7, and 2.3. From these data and the relationship between σ and the coefficient of variation for a log-normal distribution, we calculated values of σ_f, the log-normal standard deviation for flow, of 0.577, 0.954, and 1.226,

respectively. The corresponding ratios, $\sigma_f/\sigma_{\ln k}$, are 0.58, 0.56, and 0.53.

Once again, the ratio of an effective σ to the σ value used to generate the permeability distribution appears to be nearly constant, although its value in Tompson and Gelhar's study is almost twice that of Moreno and Tsang. There is no obvious reason why the results should be so different, although it should be noted that values derived from Tompson and Gelhar are based on velocity moments, while the others are based on moments of a tracer breakthrough curve generated by particle tracking. Also, the Tompson and Gelhar simulations are more highly resolved than most of the other calculations. It is possible that Moreno and Tsang's results were subject to greater numerical dispersion, which would tend to reduce the effective stratification.

Tompson and Gelhar also reported tracer breakthrough curves, although not in sufficient detail to allow calculation of σ or *Pe*. However, their breakthrough curves do show a tendency for the peaks to sharpen and move to earlier time as $\sigma_{\ln k}$ increases.

Finally, we should mention that the analytical model is expected to show the greatest sensitivity to σ, since it assumes complete stratification. We would expect the effective σ for transport to approach $\sigma_{\ln k}$ as the correlation length approaches the size of the model domain.

This entire subject warrants additional study, but there does seem to be some hope of developing, at least empirically, relatively simple relationships between effective values of σ for flow and transport and σ for the permeability distribution.

D. Variable ϕ and R

In deriving the equations for the log-normal model, we set several variables equal to their average values in order to perform the integrations. It can be shown that, if the following relationships are assumed

$$\phi = Ak^n \qquad R = Bk^m \qquad (66),$$

where A, B, n, and m are constants, then the substitution can be justified, but the integrations have to be performed over a transformed log-normal variable, with parameters simply related to the constants in Eq. (66) and the parameters of the original log-normal distribution of permeability. Once again, log-normality of the transport process is preserved, but the parameters have to be adjusted. In this case, however, the adjustment can be made rigorously within the assumptions of Eq. (66).

E. Fractal Processes

Hewett has, for about 10 years, been systematically investigating the use of fractal processes (in particular, fractional Brownian motion) to represent heterogeneity in petroleum reservoir simulations.[5] Permeability fields generated in this fashion have a very different correlation structure than is given by the usual assumption of an exponential variogram. In the latter case, correlations are essentially negligible after some multiple of the length scale, and displacements asymptotically become Fickian (although, as Matheron noted, the length and time scale may be such as to preclude this limit from ever being reached in field-scale displacements).

One characteristic of fractal behavior is that correlations appear at all scales of measurement. This implies that displacements may not become Fickian at any scale. Arya[2] gave the following expression for what he termed the megascopic dispersion coefficient:

$$\alpha_{ME} = \frac{1}{2}\frac{d\sigma_x^2}{d\bar{x}} \qquad (67),$$

along with the following equation for the variance of fractional Brownian motion:

$$\sigma_x^2 = C\bar{x}^{(4-2D_f)} \qquad (68).$$

In Eq. (68), C is a constant and D_f is the fractal dimension. From these equations, we obtain

$$\alpha_{ME} = CH\bar{x}^{2H-1} \qquad (69),$$

where $H = 2 - D_f$ is the Hurst coefficient.

When H = 1/2, the megascopic dispersivity is constant, corresponding to classical Brownian motion, and the Peclet number is proportional to the mean distance traveled. For $H \rightarrow 1$, the dispersivity becomes proportional to the mean distance traveled, and the Peclet number becomes constant. In this sense, the log-normal model represents a limiting case of fractional Brownian motion for generating the spatial distribution of ln*k*.

Hewett[5] reported a value of H = 0.87 based on well-log analysis for a more than 300 m thick section of a Pleistocene submarine fan. For this value of H, the dispersivity should be proportional to the 0.74 power of distance, according to Eq. (69).

However, when he subsequently[4] simulated miscible displacement through a two-dimensional permeability

field generated by fractional Brownian motion with H = 0.87 and plotted the mixing zone width and effective dispersion coefficients versus mean distance traveled on a log-log plot, he found that these quantities varied as the 0.991 and 0.982 powers of mean distance traveled, respectively, as noted previously in Section III. Hence, it appears that displacements behave more like the log-normal model than is predicted by Eq. (67) in that the distance exponent of effective dispersivities calculated from the simulations is much closer to unity than to 0.74.

F. Distance Scaling

As shown in Fig. 2, the general linear trend of dispersivity with the spatial scale of transport problems is well-represented by the purely advective log-normal model. However, in subsequent discussion, we showed that there is no unique relationship between dispersivity and the σ parameter, because the shapes of the breakthrough and profile curves of the log-normal model are so different from those of the CD model.

In fact, it is this author's belief that the concept of dispersivity has outlived its usefulness, and that field data might well make more sense if they were used to determine an effective σ rather than to calculate dispersivity. The former parameter seems more likely to be a property of the medium, or at least of the medium and the fluids it contains, than is the dispersivity.

VIII. SUMMARY AND CONCLUSION

In this paper, the use of the conceptual model of flow through independent, log-normally distributed linear elements is only a device for the spatial allocation of flow. The permeability serves mostly as a dummy random variable with an assumed distribution, allowing sums over the flow elements to be replaced by integrals. From this viewpoint, the parameter σ, which is introduced as the standard deviation of the natural logarithm of permeability (*i.e.*, $\sigma_{\ln k}$), becomes a parameter of the total flow and transport problem, including the nature of displacing and displaced fluids, injection/production well patterns, and so on. We have given some comparisons, based on the work of others, of the effective σ values for flow and transport to the input value used to generate the permeability field.

The work of Neretnieks, Moreno, and co-workers has generally been of a more fundamental nature, starting with the idea of flow channels within single fractures, which arise from a log-normal distribution of apertures. They are attempting to understand the mechanisms of flow and transport, including matrix diffusion, adsorption, etc., in which the underlying physical model has identifiable channels. However, their more recent investigations, including several in collaboration with Tsang and others at Lawrence Berkeley Laboratory on strongly heterogeneous media, indicate that we are converging on the same idea of using systems with a log-normal distribution to model everything from relatively homogeneous porous media to fractured rock.

It is this author's belief that this approach, as well as being simple and requiring little computing time, will provide more realistic results for modeling long-distance radionuclide transport than the current stochastic modeling approach of calculating an average flow field and then modeling transport with the average flow field and some sort of effective dispersivity. It offers, perhaps, the best hope of connecting detailed mechanistic process models with high level performance assessment models, in such a way that important parameters of the high-level models can be measured or otherwise extracted from site characterization data.

Detailed simulations, used as numerical experiments to investigate the relationship of flow and transport heterogeneity to the heterogeneity and spatial correlation structure of the rock properties, will continue to be very useful research tools, but would not directly be used in assessing the performance of Yucca Mountain as a potential site for a nuclear waste repository.

Since large values of σ appear capable of representing the phenomena associated with channeling, fast flow paths, etc., there is a good chance that we will not have to resort to models with explicit representations of fractures in order to realistically assess the long-distance transport of radionuclides away from a repository.

Finally, it seems appropriate to close with a modification of the title of Matheron and de Marsily's 1980 paper (Is Transport in Porous Media Always Diffusive?): Is it *ever*?

ACKNOWLEDGMENTS

This work was performed at Lawrence Livermore National Laboratory under the auspices of the US Department of Energy contract number W-7405-ENG-48, and was sponsored by the Yucca Mountain Site Characterization Project Office of the Office of Civilian Radioactive Waste Management (OCRWM). This financial support is gratefully acknowledged. I also appreciate receiving many stimulating reports and papers on highly resolved transport simulations and related topics

(some in draft form) from Dr. A.F.B. Tompson of LLNL. Thanks are also due to Dr. Kenneth J. Jackson for his timely review of a draft of this paper and his helpful comments.

Some of the recent developments in this approach to analyzing the effects of heterogeneity on radionuclide and tracer transport were inspired by the author's participation in the OCRWM International Programs as a member of several scientific advisory groups and as an investigator in the joint US/Swedish program at the Äspö Hard Rock Laboratory.

I would particularly like to thank Dr. Robert A. Levich for supporting these activities. Also, I am especially grateful to Professors Ivars Neretnieks and Luis Moreno of the Royal Institute of Technology in Stockholm for stimulating discussions of related work in December 1993. In particular, I would like to thank Professor Moreno for supplying a preprint of his and Dr. Chen-Fu Tsang's paper on strongly heterogeneous systems which will be published in 1994, and Professor Neretnieks for assembling a set of reprints of his work for me.

NOMENCLATURE

Unless otherwise noted in the text, all variables are given in MKS units. The following list is approximately in the order in which the symbols were first used.

t	time
t_b	mean breakthrough time
τ	dimensionless time
σ	log-normal standard deviation
p	a real number
x	distance of contaminant travel
$\langle x \rangle$	the mean of x
$\langle\rangle$	denotes the mean of any variable enclosed by the brackets
x_m	median distance traveled
η	dimensionless distance
q	volumetric flow rate
P	pressure
A	Area
L	length
k	permeability
μ	viscosity
u	Darcy flux (volumetric flow rate per unit area)
v	fluid velocity
ϕ	fractional porosity
K	volumetric sorption coefficient
R	retardation factor
$f(k)$	probability density function for k
c_0	concentration at the injection boundary
$c(x,t)$	concentration at distance x from the inlet and time t after beginning injection
ξ	normalized concentration
$\Phi(z)$	normal probability integral of z
α	dispersivity
Pe	Peclet number
$\mathrm{erfc}(u)$	complementary error function of u
W	width of an apparent mixing zone
ω	dimensionless width of an apparent mixing zone
$\sinh(u)$	hyperbolic sine of u
γ	dimensionless mean distance traveled for small values of Pe, from CDE solution
m_p	the p^{th} moment of the breakthrough time distribution
CV	coefficient of variation

REFERENCES

1. I. Javendel, C. Doughty, and C.F. Tsang, *Groundwater Transport: Handbook of Mathematical Models, Water Resources Monograph 10*, American Geophysical Union, Washington, DC (1984).

2. Atul Araya, Tom A. Hewett, Ronald G. Larson, and Larry W. Lake, "Dispersion and Reservoir Heterogeneity," *SPE Reservoir Engineering*, Feb., pp. 139-148 (1988).

3. G. Matheron and G. de Marsily, "Is Transport in Porous Media Always Diffusive? A Counterexample," *Water Resources Research* **16**, #5, pp. 901-917, October (1980).

4. T.A. Hewett and R. A. Behrens, "Considerations Affecting the Scaling of Displacements in Heterogeneous Permeability Distributions," *SPE 65th Annual Technical Conference*, New Orleans, LA, September 23-26, 1990, Preprint 20739, pp. 233-241, Society of Petroleum Engineers, Richardson, TX, (1990).

5. T.A. Hewett, "Fractal Distributions of Reservoir Heterogeneity and Their Influence on Fluid Transport," *SPE 61st Annual Technical Conference*, New Orleans, LA, October 5-8, 1986, Preprint 15386,

Society of Petroleum Engineers, Richardson, TX, (1986).

6. D.A. Chesnut, D.O. Cox, and G. Lasaki. "A Practical Method for Waterflood Performance Prediction and Evaluation," *Proc. edings, Pan American Congress of Petroleum Engineering*, Mexico City, 1979.

7. Dwayne A. Chesnut, *A Dispersion Model for Chemical Flooding*, Shell Oil Company, Western Region, Production Department, Denver, CO, November, 1970.

8. D.A. Chesnut, "Characterizing the Altered Zone at Yucca Mountain: The Beginning of a Testing Strategy," *Proceedings, Third International High-Level Radioactive Waste Management Conference*; American Nuclear Society, Inc.: Las Vegas, NV, pp. 1026-1039 (1992).

9. D.A. Chesnut, "Heterogeneity and Vapor Extraction Performance," in *Emerging Technologies in Hazardous Waste Extraction IV*, American Chemical Society Symposium Series American Chemical Society, Washington, DC, 1994 (in press).

10. Ivars Neretnieks, "A Note on Fracture Flow Dispersion Mechanisms in the Ground," *Water Resources Research* 19, April, pp. 364-370, (1983).

11. Greg L. Butters, William A. Jury, and Frederick L. Ernst, "Field Scale Transport of Bromide in Unsaturated Soil. 1. Experimental Methodology and Results," *Water Resources Research* 25, #7, pp. 1575-1581, July (1989).

12. Greg L. Butters and William A. Jury, "Field Scale Transport of Bromide in Unsaturated Soil. 2. Dispersion Modeling," Water Resources Research 25, #7, pp. 1583-1589, July (1989).

13. William A. Jury and G. Sposito, "Field Calibration and Validation of Solute Transport Models for the Unsaturated Zone," *Soil Sci. Soc. Am. J.* 49, 1331-1341 (1985).

14. A.F.B. Tompson and D.E. Dougherty, *Highly Resolved Simulations of Chemical Migration in Physically and Chemically Heterogeneous Porous Media*, Lawrence Livermore National Laboratory, UCRL-JC-109629, February (1992).

15. Ivars Neretnieks, Tryggve Eriksen, and Päivi Tähtinen, "Tracer Movement in a Single Fissure in Granitic Rock: Some Experimental Results and Their Interpretation," *Water Resources Research*, Aug., pp. 849-858 (1982).

16. Atul Arya, *Dispersion and Reservoir Heterogeneity*, Ph.D. Dissertation, U. of Texas, Austin (1986).

17. J.F. Pickens and G.E. Grisak, "Scale-Dependent Dispersion in a Stratified Granular Aquifer," *Water Resources Research*, Apr., pp. 1191-1211 (1981).

18. A. Lallemand-Barrès and P. Peaucederf, "Recherche des relations entre le valeur de la dispersivité macroscopique d'un milieu aquifère, ses autres caractéristiques et les conditions de mesure," *Bull., BRGM 2e Serie, Sec. III*, No. 4 (1978).

19. Luis Moreno, Ivars Neretnieks, and Tryggve Eriksen, "Analysis of Some Laboratory Tracer Runs in Natural Fissures," *Water Resources Research* 21, #7, pp. 951-958, July (1985).

20. O. Levenspiel, *Chemical Reaction Engineering*, 2nd. ed., John Wiley, New York, 1972.

21. Luis Moreno and Chin-Fu Tsang, "Flow Channeling in Strongly Heterogeneous Porous Media: A Numerical Study," *Water Resources Research*, (in press, 1994)

22. P.C. Robinson, Connectivity, Flow, and Transport in Network Models of Fractured Media, Ph.D. Thesis, St. Catherine's College, Oxford University, Ref TP 1072, May 1984.

23. A.F.B. Tompson and Lynn W. Gelhar, "Numerical Simulation of Solute Transport in Three-Dimensional, Randomly Heterogeneous Porous Media," *Water Resources Research* 26, #10, pp. 2541-2562, October (1990).

DATE
FILMED
7/1/94
END